Multipartite Entanglement in a Microwave Frequency Comb

Multipartite Entanglement in a Microwave Frequency Comb

Shan W. Jolin,[1,*,†] Gustav Andersson,[2,3] J. C. Rivera Hernández,[1] Ingrid Strandberg,[3] Fernando Quijandría,[3,‡] José Aumentado,[4] Riccardo Borgani,[1,5] Mats O. Tholén,[1,5] and David B. Haviland[1]

[1]*Department of Applied Physics, KTH Royal Institute of Technology, SE-106 91 Stockholm, Sweden*
[2]*Pritzker School of Molecular Engineering, University of Chicago, Chicago, Illinois 60637, USA*
[3]*Department of Microtechnology and Nanoscience MC2, Chalmers University of Technology, SE-412 96 Göteborg, Sweden*
[4]*National Institute of Standards and Technology, 325 Broadway, Boulder, Colorado 80305, USA*
[5]*Intermodulation Products AB, SE-823 93 Segersta, Sweden*

(Received 22 December 2021; accepted 23 February 2023; published 23 March 2023)

Significant progress has been made with multipartite entanglement of discrete qubits, but continuous variable systems may provide a more scalable path toward entanglement of large ensembles. We demonstrate multipartite entanglement in a microwave frequency comb generated by a Josephson parametric amplifier subject to a bichromatic pump. We find 64 correlated modes in the transmission line using a multifrequency digital signal processing platform. Full inseparability is verified in a subset of seven modes. Our method can be expanded to generate even more entangled modes in the near future.

DOI: 10.1103/PhysRevLett.130.120601

Superconducting quantum circuits have demonstrated excellent unitary control and coherence of qubits at a level sufficient to usher in the era of noisy intermediate-scale quantum technologies [1]. So far, a vast majority of the research is focused on the circuit-based approach to quantum computing [2]. An alternative paradigm is the measurement-based one-way quantum computer [3–5], where computation is realized through a sequence of measurements on so-called cluster states [6,7]. This paradigm has received significantly more attention in optics, where the continuous variable (CV) counterpart has revealed large scale multipartite entanglement in optical frequency combs involving many thousands of modes [8–13].

Ever since the pioneering experiments of Yurke *et al.* [14,15], single and two-mode squeezing has been observed in a wide variety of systems, from superconducting [16–27] to mechanical [28–30]. However, to generate an arbitrary cluster state, multimodal squeezing [31] beyond two modes is required. Tripartite squeezing has been demonstrated in superconducting devices [32–34] and multimode squeezing has been demonstrated with parametrically coupled surface acoustic wave modes [35]. But large multipartite entanglement in the microwave spectrum with superconducting circuits remains elusive.

In this Letter we demonstrate squeezing of multiple propagating modes in a transmission line connected to a Josephson parametric amplifier (JPA) with a bichromatic pump. Our digital signal processing platform enables measurements of correlations between as many as 64 modes. While genuine multipartite entanglement between so many modes is nontrivial to establish unequivocally [36–39], we present compelling evidence of seven fully inseparable modes. Our method provides a clear path for scaling to many more modes and perhaps construction of CV cluster states.

Our JPA is a lumped-element LC circuit (see Fig. 1) cooled to 10 mK, where the inductor is replaced by a superconducting quantum interference device (SQUID). The JPA is overcoupled at the signal port to a circulator which separates incoming and outgoing modes in two transmission lines, with the outgoing modes connected through a double isolator to a cryogenic low-noise amplifier. The second port is inductively coupled to the SQUID loop, through which we apply a time-varying flux pump to modulate the circuit inductance. The flux pump together with the flux bias permit a three-wave mixing process, known to amplify small signals and generate two-mode squeezing [40]. The overcoupled linewidth of the JPA resonance is $\kappa_{\text{total}} = 2\pi \times 124$ MHz.

Noise quadrature data are collected by a digital multifrequency lock-in that simultaneously demodulates at many frequencies, each being an integer multiple of the measurement bandwidth. We measure the *IQ* quadratures of up to 64 evenly spaced frequencies with no Fourier leakage between the demodulated frequencies. The measurement is facilitated by directly digitizing in the second Nyquist zone, granting access to the 2.5–5 GHz band without analog

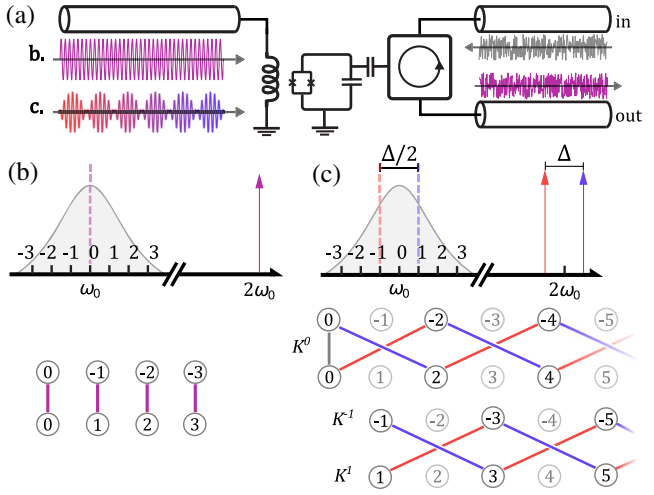

FIG. 1. (a) The JPA forms a LC circuit with tunable inductance L_J due to the SQUID. The inductance, and hence its resonance frequency ω_0, is modulated by an external flux field of the monochromatic or bichromatic kind, labeled **b** and **c**, respectively. The pump stimulates incoming vacuum noise scattering off the JPA resonance to become entangled (right). The incoming and outgoing noise is separated by a circulator. (b) A monochromatic flux pump is applied at $\omega_p \approx 2\omega_0$, which correlates modes symmetrically around mode 0. We use a graph to indicate the resulting correlations in the frequency comb. Numbered vertices correspond to labels on the frequency axis and edges indicate classical or quantum correlations. (c) A bichromatic flux pump consists of two different frequencies at roughly $2\omega_0$. We can illustrate the correlations with graphs K^0, K^{-1}, and K^1. The superscript indicates the root vertex. In our Letter, $\Delta = 2\pi \times 9.2$ MHz and $\omega_0 \approx 2\pi \times 4.3$ GHz.

mixers. Analog bandpass filters at the lock-in input reduce the effect of aliasing. The digital multifrequency lock-in's clock is the reference oscillation for our external microwave generator which supplies the flux pump. For additional details, see the Supplemental Material [41], which includes Refs. [42–64].

The frequencies at which we measure and demodulate, the modes, are determined by the flux pump frequencies. A bichromatic pump, with frequencies Ω_1 and Ω_2, is applied at the flux bias port. The frequencies are approximately centered at twice the JPA resonance $\frac{1}{2}(\Omega_2 + \Omega_1) \approx 2\omega_0$ with a detuning Δ smaller than the JPA linewidth, $|\Omega_2 - \Omega_1| = \Delta \ll \kappa_{\text{total}}$. Measurement is carried out at a comb of frequencies $f_n = \frac{1}{4}(\Omega_2 + \Omega_1) + n\Delta/4$, $n \in \mathcal{Z}$, with spacing $\Delta/4$ [see Fig. 1(c)]. This particular frequency selection ensures that signal-idler pairs associated with each pump overlap, giving rise to multimode squeezing. In our experiments we use $\Delta = 2\pi \times 9.2$ MHz for the pumps and $\Delta/4 = 2\pi \times 2.3$ MHz for the frequency comb.

To help visualize the correlations induced by pumping, we first consider the familiar case of a monochromatic pump, as illustrated in Fig. 1(b). Every frequency in the comb is labeled by an integer, with 0 signifying the center frequency $(\Omega_1 + \Omega_2)/4$. In the three-wave mixing process $2\omega_0 = \omega_n + \omega_{-n}$, correlations arise between signal-idler pairs labelled n and $-n$. A graph represents the correlations, where vertices indicate comb frequencies and edges connect signal-idler pairs satisfying the three-wave mixing criterion. We find that all vertices (except vertex 0) have only one incident edge. These vertices are said to be of degree 1 and correspond to two-mode squeezing. Note that vertex 0 is unique since it is single-mode squeezed and has an edge to itself, i.e., self-loop.

Going beyond two-mode squeezing requires vertices of higher degree and preferably without self-loops. We achieve this with a bichromatic pump, as shown in Fig. 1(c). We partition the entire comb into three infinitely long subgraphs K^0, K^1, and K^{-1}. The superscripts indicate the root vertices, defined as the leftmost vertex in Fig. 1(c). The edges are color coded to indicate which pump facilitates the interaction. The graphs for two pumps suggest that a photon detected in any mode could be correlated with an idler at another mode via either the red pump or the blue pump. This ambiguity about exactly which photons are involved in two-mode squeezing can be viewed as an absence of which-color information [34,65], in analogy to the absence of which-path information required to entangle spatially separated photons [66].

We sample the noise output from the flux pumped JPA to construct the measured covariance matrix $\tilde{C}_{nm} = \langle (A_n - \langle A_n \rangle)(A_m - \langle A_m \rangle) \rangle$, where $A_n \in \{I_n, Q_n\}$ is the measured quadrature value for mode n. The measured matrix $\tilde{C}_{nm}$ (obtained in units of V^2) is scaled according to

$$\tilde{V}_{nm} = \frac{\tilde{C}_{nm}}{\frac{1}{2}\sqrt{\omega_n \omega_m} Z_c \hbar B}, \tag{1}$$

where ω_n (ω_m) denotes the frequency of mode n (m), while Z_c, B and $\hbar$ are the characteristic impedance of the line (50 Ω), the measurement bandwidth (1 kHz) and Planck constant, respectively. This scaling permits the covariance matrix to be stated in units of twice the photon number ($2\bar{n}$) and the vacuum state as the identity matrix. $\tilde{V}_{nm}$ is subsequently compensated for the frequency-dependent gain and added noise of the amplifier chain using a procedure documented in the Supplemental Material [41]. The result is a calibrated covariance matrix V'_{nm}.

A physical covariance matrix must be semi-positive definite and it must not violate the uncertainty principle. For a general covariance matrix V in our units, we express these conditions as [67]

$$V \geq 0, \qquad V - i\Omega \geq 0, \tag{2}$$

with the symplectic matrix $\Omega = \bigotimes_n \left(\begin{smallmatrix} 0 & 1 \\ -1 & 0 \end{smallmatrix}\right)$.

When compensating the measured covariance matrix $\tilde{V}_{nm}$ for added measurement noise, it may happen that the calibrated covariance matrix V'_{nm} violates Eqs. (2).

Therefore, we constrain this compensation to reconstruct a physical covariance matrix, within experimental error σ_{nm}, that does satisfy Eqs. (2), by minimizing the objective function [68]

$$\min_{V}\left(\max_{nm}\frac{|V'_{nm}-V_{nm}|}{\sigma_{nm}}\right). \tag{3}$$

Ideally the objective function should be less than unity for a plausible reconstruction (i.e., the reconstructed matrix is within experimental error of the calibrated matrix). With this reconstructed covariance matrix, we proceed to analyze the entanglement properties.

We first test for entanglement generated by a monochromatic flux pump, (−3 dBm output power) well known to generate pairs of entangled modes, known as two-mode squeezed states [16–27]. We measure the covariance matrix of the closest seven modes around the half-pump frequency with 1 kHz measurement bandwidth, acquiring 6×10^5 data points over 10 min. To minimize the effect of phase drift in this long-time measurement, we divide the dataset into six equal segments. Reconstructing a physical covariance matrix in each segment, we find a maximum deviation 4×10^{-5} σ from the calibrated matrix. We present one of these covariance matrices in Fig. 2(a). The 0 mode is located at exactly half the pump frequency. Consequently, all modes symmetric around the 0 mode create two-mode squeezed states, as indicated by the checkered blue-red antidiagonal. The three pairs are analyzed for entanglement using the PPT test [69] and the Duan criterion [70]. The weighted results for the six matrices are presented in Fig. 2(b). Analysis indicates the three pairs exhibit bipartite entanglement. See the Supplemental Material [41] for details.

As depicted in the graphs of Fig. 1, a monochromatic pump generates only bipartite states which are either entangled or separable. In contrast, a bichromatic pump generates a multipartite state which may belong to one of many possible entanglement and separability classes—ranging from *fully separable* to *genuinely multipartite entangled* (GME). As a generalization of the bipartite case, a n-partite ($n>2$) mixed state is fully separable if it can be written as a convex combination of product states. Furthermore, an n-partite state can be arranged into $k\le n$ partitions. If the state is fully separable with respect to k partitioning (or expressed as a mixture of k partitions), we call it *k-separable*, if not, *k-inseparable* [71]. We call the n-partite state *fully inseparable* if it is not separable with respect to any partitioning [72]. Additional details are given in the Supplemental Material [41].

To establish whether an n-mode state is fully inseparable, it suffices to establish that the state in question is inseparable with respect to any bipartitioning, i.e., it exhibits bi-inseparability. For pure states, bi-inseparability is a necessary and sufficient condition for GME, as it implies entanglement for any other k partitioning of modes. However for mixed states, bi-inseparability substantiates only the claim of full inseparability [73]. To establish the latter we test for entanglement on all possible bipartitions of the n-mode state; a computationally demanding task that grows exponentially with the number of modes n (the number of bipartitions is $2^{n-1}-1$).

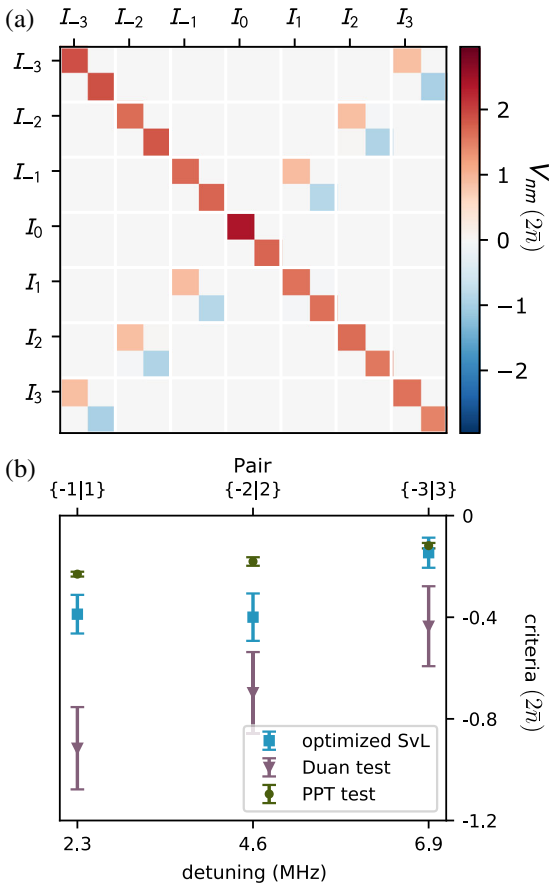

FIG. 2. (a) Reconstructed covariance matrix generated by a monochromatic pump. The mode at the half-pump frequency is visible at the center where the red diagonal and the red-blue antidiagonal intersect. The red diagonal contains noise, while the red-blue antidiagonal indicates pairwise correlations. For clarity, only the I quadratures are labeled on the x and y axes. The Q quadratures are interleaved between I columns and rows. The subscripts label different modes. The covariance matrix is given in units of twice the photon number $2\bar{n}$. (b) Each mode-pair symmetric around the half-pump frequency 4.3 GHz is analyzed for entanglement using the PPT test [69], the Duan criterion [70], and a SvL test [37,68] using optimization; see Eq. (4). With our convention, non-negative values correspond to separable states. All three tests return negative results. The bottom x axis indicates the detuning between mode $n\in[\pm1,\pm2,\pm3]$ and the half-pump frequency mode. Because of our choice of covariance matrix normalization, the criteria are consequently given in units of twice the photon number. The error bars and values are the weighted mean and uncertainties (1 standard deviation) from an ensemble of six measurements lasting 10 min each.

We use a bipartition test developed by Shchukin and van Loock [37,68], henceforth referred to as the SvL test. Consider the case of a covariance matrix V with zero IQ correlations (or, equivalently, zero xp correlations [67]). This state is equally well characterized by two smaller matrices V^{II} and V^{QQ} containing only II and QQ correlations respectively, a reduction which is always possible with local Gaussian transformations such as single mode phase rotations. Local Gaussian transformations can only transform entangled states into other entangled states, and separable states into other separable states [70]. If n modes are divided into bipartitions $\mathcal{I}$ and $\mathcal{J}$, then the SvL condition for separability between $\mathcal{I}$ and $\mathcal{J}$ reads [68]

$$\mathcal{E} = \mathrm{Tr}[V^{II}(\boldsymbol{h}\otimes\boldsymbol{h})] + \mathrm{Tr}[V^{QQ}(\boldsymbol{g}\otimes\boldsymbol{g})] - 2|\langle h_{\mathcal{I}}, g_{\mathcal{I}}\rangle| - 2|\langle h_{\mathcal{J}}, g_{\mathcal{J}}\rangle| \geq 0, \tag{4}$$

where $\boldsymbol{h}$ and $\boldsymbol{g}$ are arbitrary real valued vectors with lengths n, and each element is assigned to every mode. Depending on whether the mode belongs to the $\mathcal{I}$ or $\mathcal{J}$ partition, we extract the corresponding elements from $\boldsymbol{h}$ and $\boldsymbol{g}$ to create vectors $h_{\mathcal{I}}$, $g_{\mathcal{I}}$ and $h_{\mathcal{J}}$, $g_{\mathcal{J}}$. For example, consider three modes $\{1,2,3\}$ and the vectors $\boldsymbol{h} = (h_1, h_2, h_3)^{\intercal}$, $\boldsymbol{g} = (g_1, g_2, g_3)^{\intercal}$. If the bipartition is $\{\mathcal{I}|\mathcal{J}\} = \{1|2,3\}$, then we have $h_{\mathcal{I}} = (h_1)$, $g_{\mathcal{I}} = (g_1)$ and $h_{\mathcal{J}} = (h_2, h_3)^{\intercal}$, $g_{\mathcal{J}} = (g_2, g_3)^{\intercal}$.

If the bipartition is separable, then the inequality Eq. (4) holds for all $\boldsymbol{h}$ and $\boldsymbol{g}$. Thus, bi-inseperability is established if we find at least one pair of vectors $\boldsymbol{h}$ and $\boldsymbol{g}$ which violates the inequality, i.e., for which $\mathcal{E}$ is negative, in each possible bipartition. To check for consistency with other entanglement tests we apply the SvL test to the monochromatic pump data with the result shown in Fig. 2(b). The vectors $\boldsymbol{h}$ and $\boldsymbol{g}$ are optimized to minimize the ratio $\mathcal{E}/\delta\mathcal{E}$, where $\delta\mathcal{E}$ is the uncertainty in $\mathcal{E}$. From Fig. 2(b), it is clear that all three tests agree on the states' entangled character.

We use the SvL test to demonstrate our main result: the generation of a fully inseparable multipartite state with a bichromatic pump. Figure 3 shows the measured covariance matrix of 64 modes generated by a bichromatic flux-pump each with −7 dBm output power (left). The measurement is qualitatively well reproduced by our theory (right) provided in the Supplemental Material [41]. With 64 frequencies the number of possible bipartitions exceeds 9×10^{18}. This number is reduced by exploiting the connection topology shown in Fig. 1. We divide the covariance matrix into the three smaller subsets of modes: K^0, K^{-1}, and K^1, analyzing each separately and thereby reducing the number of modes to 32 for K^0 and 16 modes for $K^{\pm 1}$. But the number of possible bipartitions remains large, roughly 2×10^9 and 32767 respectively. We therefore analyze an even smaller subset: the seven center modes in the K^0 set (K^0 modes $\in \{0, \pm 2, \pm 4, \pm 6\}$, and four modes in the

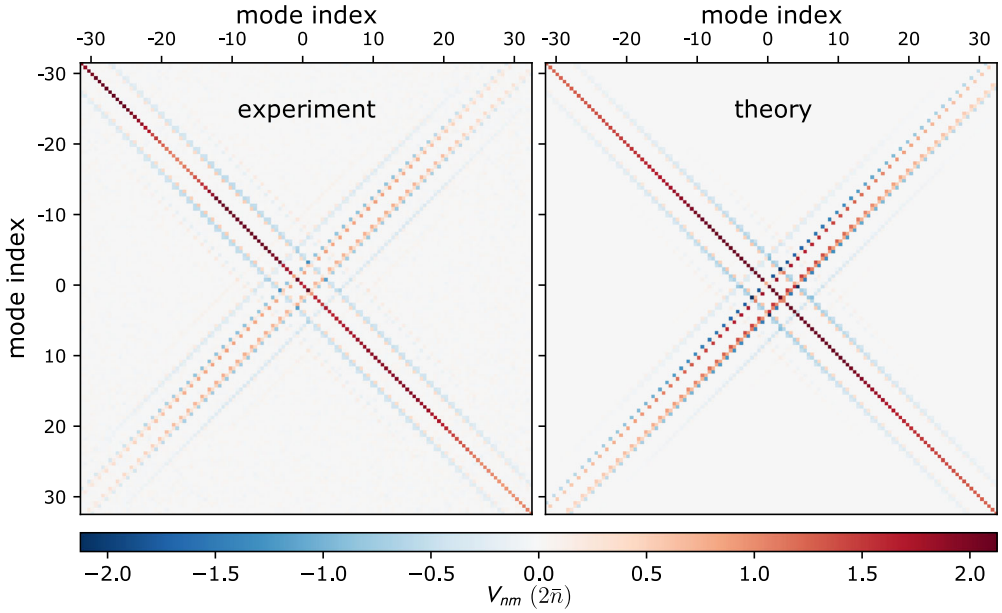

FIG. 3. Experimental covariance matrix reconstructed from measurement of 64 modes generated by two pumps (left). The presence of off-diagonals indicates at least the presence of classical correlations. To determine whether these are quantum correlations requires further analysis outlined in the main text. Our theory reproduces a qualitatively similar matrix (right). The finite bandwidth of the JPA weakens correlations among modes at the edges of the frequency comb. For clarity, we omit I and Q labels on the x and y axes. Instead they are labeled by the mode index, such that mode 0 lies at exactly half of the average pump frequency, cf. Fig. 1(c). Each mode is spaced by 2.3 MHz. Covariance matrix elements are given in units of twice the photon number ($2\bar{n}$), making the identity matrix correspond to the vacuum state.

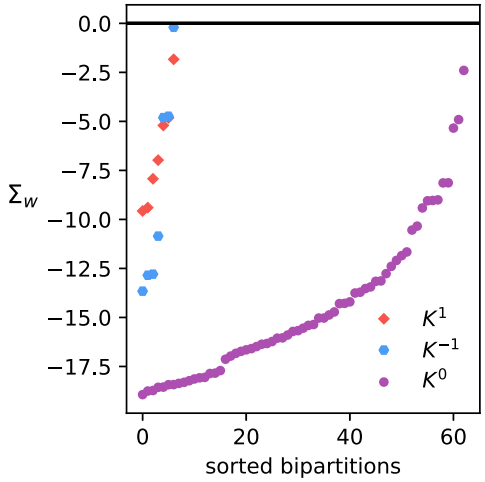

FIG. 4. Bipartition test for the seven center modes in the K^0 set and four center modes from $K^{\pm 1}$. For K^0, all tests violate the requirement for separability by at least 2.5 standard deviations, indicating that we have strong evidence for full inseparability. For K^1, we have full inseparability with a significance of 2 standard deviations. However evidence for full inseparability for the K^{-1} set is significantly weaker.

$K^{\pm 1}$-sets (K^{-1} modes $\in \{-5, -1, 3, 7\}$ and K^1 modes $\in \{-7, -3, 1, 5\}$).

As for the monochromatic pump case, we divide a 10 min measurement with 1 kHz bandwidth into six segments, reconstructing the covariance matrix in each, with maximum deviation of 1.15σ, 0.95σ, and 0.92σ for subsets K^{-1}, K^0, and K^1, respectively. We perform the SvL test Eq. (4) on each matrix of each subset, with vectors $\boldsymbol{h}$ and $\boldsymbol{g}$ that are individually optimized to minimize $\mathcal{E}/\delta\mathcal{E}$.

The results are summarized in Fig. 4 as a weighted mean entanglement significance $\Sigma_w = \mathcal{E}_w/\delta\mathcal{E}_w$ ($\mathcal{E}_w$ is the mean and $\delta\mathcal{E}_w$ is the corresponding uncertainty). For example, if $\Sigma_w = -5$, entanglement is established with a statistical significance of 5 standard deviations. Since all bipartitions violate the inequality Eq. (4) by at least 2.5 standard deviations, we have substantial evidence for full inseparability of seven modes. We probably have full inseparability for four modes in K^1, while evidence for K^{-1} is weaker.

In conclusion, direct digital modulation and demodulation methods provide a powerful tool for generation of multipartite entanglement in a microwave frequency comb. We demonstrated this with 64 modes using a bichromatic pump and used the SvL test to show full inseparability of a subset of 7 modes in the comb. A direct extension of our technique should allow for the creation of multimodal Gaussian cluster states through precise control of the amplitude and phase of the multiple pumps [74]. For example, pumping at $2\omega_0$ in combination with pumping at the comb spacing $\Delta/2$, should control the scattering between nearest neighbour modes, as in Ref. [75]. Other possible applications include quantum simulation [76,77] and reservoir computing with continuous variable Gaussian states [78].

We acknowledge fruitful discussions with Giulia Ferrini and support by the Knut and Alice Wallenberg Foundation through the Wallenberg Center for Quantum Technology (WACQT). R. B., M. O. T., and D. B. H. are part owners of the company Intermodulation Products AB, which produces the digital microwave platform used in this experiment.

*shan@meetiqm.com
†Present address: IQM Finland Oy, Espoo 02150, Finland.
‡Present address: Quantum Machines Unit, Okinawa Institute of Science and Technology Graduate University, Onna-son, Okinawa 904-0495, Japan.

[1] F. Arute *et al.*, Quantum supremacy using a programmable superconducting processor, Nature (London) **574**, 505 (2019).
[2] M. A. Nielsen and I. L. Chuang, *Quantum Computation and Quantum Information* (Cambridge University Press, Cambridge, England, 2000).
[3] R. Raussendorf and H. J. Briegel, A One-Way Quantum Computer, Phys. Rev. Lett. **86**, 5188 (2001).
[4] R. Raussendorf, D. E. Browne, and H. J. Briegel, Measurement-based quantum computation on cluster states, Phys. Rev. A **68**, 022312 (2003).
[5] M. V. Larsen, J. S. Neergaard-Nielsen, and U. L. Andersen, Architecture and noise analysis of continuous-variable quantum gates using two-dimensional cluster states, Phys. Rev. A **102**, 042608 (2020).
[6] H. J. Briegel and R. Raussendorf, Persistent Entanglement in Arrays of Interacting Particles, Phys. Rev. Lett. **86**, 910 (2001).
[7] N. C. Menicucci, P. van Loock, M. Gu, C. Weedbrook, T. C. Ralph, and M. A. Nielsen, Universal Quantum Computation with Continuous-Variable Cluster States, Phys. Rev. Lett. **97**, 110501 (2006).
[8] J. Roslund, R. M. de Araújo, S. Jiang, C. Fabre, and N. Treps, Wavelength-multiplexed quantum networks with ultrafast frequency combs, Nat. Photonics **8**, 109 (2014).
[9] O. Pfister, Continuous-variable quantum computing in the quantum optical frequency comb, J. Phys. B **53**, 012001 (2019).
[10] S. Yokoyama, R. Ukai, S. C. Armstrong, C. Sornphiphatphong, T. Kaji, S. Suzuki, J.-i. Yoshikawa, H. Yonezawa, N. C. Menicucci, and A. Furusawa, Ultra-large-scale continuous-variable cluster states multiplexed in the time domain, Nat. Photonics **7**, 982 (2013).
[11] J.-i. Yoshikawa, S. Yokoyama, T. Kaji, C. Sornphiphatphong, Y. Shiozawa, K. Makino, and A. Furusawa, Invited article: Generation of one-million-mode continuous-variable cluster state by unlimited time-domain multiplexing, APL Photonics **1**, 060801–11 (2016).
[12] M. V. Larsen, X. Guo, C. R. Breum, J. S. Neergaard-Nielsen, and U. L. Andersen, Deterministic generation of a two-dimensional cluster state, Science **366**, 369 (2019).

[13] W. Asavanant, Y. Shiozawa, S. Yokoyama, B. Charoensombutamon, H. Emura, R. N. Alexander, S. Takeda, J. ichi Yoshikawa, N. C. Menicucci, H. Yonezawa, and A. Furusawa, Generation of time-domain-multiplexed two-dimensional cluster state, Science **366**, 373 (2019).

[14] B. Yurke, P. G. Kaminsky, R. E. Miller, E. A. Whittaker, A. D. Smith, A. H. Silver, and R. W. Simon, Observation of 4.2-k Equilibrium-Noise Squeezing via a Josephson-Parametric Amplifier, Phys. Rev. Lett. **60**, 764 (1988).

[15] R. Movshovich, B. Yurke, P. G. Kaminsky, A. D. Smith, A. H. Silver, R. W. Simon, and M. V. Schneider, Observation of Zero-Point Noise Squeezing via a Josephson-Parametric Amplifier, Phys. Rev. Lett. **65**, 1419 (1990).

[16] E. A. Tholén, A. Ergül, K. Stannigel, C. Hutter, and D. B. Haviland, Parametric amplification with weak-link nonlinearity in superconducting microresonators, Phys. Scr. **2009**, 014019 (2009).

[17] C. Eichler, D. Bozyigit, C. Lang, M. Baur, L. Steffen, J. M. Fink, S. Filipp, and A. Wallraff, Observation of Two-Mode Squeezing in the Microwave Frequency Domain, Phys. Rev. Lett. **107**, 113601 (2011).

[18] M. A. Castellanos-Beltran, K. D. Irwin, G. C. Hilton, L. R. Vale, and K. W. Lehnert, Amplification and squeezing of quantum noise with a tunable Josephson metamaterial, Nat. Phys. **4**, 929 (2008).

[19] E. Flurin, N. Roch, F. Mallet, M. H. Devoret, and B. Huard, Generating Entangled Microwave Radiation Over Two Transmission Lines, Phys. Rev. Lett. **109**, 183901 (2012).

[20] C. Eichler, Y. Salathe, J. Mlynek, S. Schmidt, and A. Wallraff, Quantum-Limited Amplification and Entanglement in Coupled Nonlinear Resonators, Phys. Rev. Lett. **113**, 110502 (2014).

[21] C. M. Wilson, G. Johansson, A. Pourkabirian, M. Simoen, J. R. Johansson, T. Duty, F. Nori, and P. Delsing, Observation of the dynamical casimir effect in a superconducting circuit, Nature (London) **479**, 376 (2011).

[22] E. P. Menzel, R. Di Candia, F. Deppe, P. Eder, L. Zhong, M. Ihmig, M. Haeberlein, A. Baust, E. Hoffmann, D. Ballester, K. Inomata, T. Yamamoto, Y. Nakamura, E. Solano, A. Marx, and R. Gross, Path Entanglement of Continuous-Variable Quantum Microwaves, Phys. Rev. Lett. **109**, 250502 (2012).

[23] P. Lähteenmäki, G. S. Paraoanu, J. Hassel, and P. J. Hakonen, Dynamical casimir effect in a Josephson metamaterial, Proc. Natl. Acad. Sci. U.S.A. **110**, 4234 (2013).

[24] B. H. Schneider, A. Bengtsson, I. M. Svensson, T. Aref, G. Johansson, J. Bylander, and P. Delsing, Observation of Broadband Entanglement in Microwave Radiation from a Single Time-Varying Boundary Condition, Phys. Rev. Lett. **124**, 140503 (2020).

[25] M. Perelshtein, K. Petrovnin, V. Vesterinen, S. H. Raja, I. Lilja, M. Will, A. Savin, S. Simbierowicz, R. Jabdaraghi, J. Lehtinen, L. Grönberg, J. Hassel, M. Prunnila, J. Govenius, S. Paraoanu, and P. Hakonen, Broadband continuous variable entanglement generation using kerr-free Josephson metamaterial, arXiv:2111.06145.

[26] M. Esposito, A. Ranadive, L. Planat, S. Leger, D. Fraudet, V. Jouanny, O. Buisson, W. Guichard, C. Naud, J. Aumentado, F. Lecocq, and N. Roch, Observation of Two-Mode Squeezing in a Traveling Wave Parametric Amplifier, Phys. Rev. Lett. **128**, 153603 (2022).

[27] J. Y. Qiu, A. Grimsmo, K. Peng, B. Kannan, B. Lienhard, Y. Sung, P. Krantz, V. Bolkhovsky, G. Calusine, D. Kim, A. Melville, B. M. Niedzielski, J. Yoder, M. E. Schwartz, T. P. Orlando, I. Siddiqi, S. Gustavsson, K. P. O'Brien, and W. D. Oliver, Broadband squeezed microwaves and amplification with a Josephson traveling-wave parametric amplifier, Nat. Phys. (2023).

[28] T. Palomaki, J. Teufel, R. Simmonds, and K. Lehnert, Entangling mechanical motion with microwave fields, Science **342**, 710 (2013).

[29] C. F. Ockeloen-Korppi, E. Damskägg, J.-M. Pirkkalainen, T. T. Heikkilä, F. Massel, and M. A. Sillanpää, Noiseless Quantum Measurement and Squeezing of Microwave Fields Utilizing Mechanical Vibrations, Phys. Rev. Lett. **118**, 103601 (2017).

[30] S. Kotler, G. A. Peterson, E. Shojaee, F. Lecocq, K. Cicak, A. Kwiatkowski, S. Geller, S. Glancy, E. Knill, R. W. Simmonds, J. Aumentado, and J. D. Teufel, Direct observation of deterministic macroscopic entanglement, Science **372**, 622 (2021).

[31] S. Zippilli and D. Vitali, Possibility to generate any gaussian cluster state by a multimode squeezing transformation, Phys. Rev. A **102**, 052424 (2020).

[32] C. W. Sandbo Chang, M. Simoen, J. Aumentado, C. Sabín, P. Forn-Díaz, A. M. Vadiraj, F. Quijandría, G. Johansson, I. Fuentes, and C. M. Wilson, Generating Multimode Entangled Microwaves with a Superconducting Parametric Cavity, Phys. Rev. Appl. **10**, 044019 (2018).

[33] A. Agustí, C. W. Sandbo Chang, F. Quijandría, G. Johansson, C. M. Wilson, and C. Sabín, Tripartite Genuine Non-Gaussian Entanglement in Three-Mode Spontaneous Parametric Down-Conversion, Phys. Rev. Lett. **125**, 020502 (2020).

[34] P. Lähteenmäki, G. S. Paraoanu, J. Hassel, and P. J. Hakonen, Coherence and multimode correlations from vacuum fluctuations in a microwave superconducting cavity, Nat. Commun. **7**, 1 (2016).

[35] G. Andersson, S. W. Jolin, M. Scigliuzzo, R. Borgani, M. O. Tholén, J. C. Rivera Hernández, V. Shumeiko, D. B. Haviland, and P. Delsing, Squeezing and multimode entanglement of surface acoustic wave phonons, PRX Quantum **3**, 010312 (2022).

[36] J. Sperling and W. Vogel, Multipartite Entanglement Witnesses, Phys. Rev. Lett. **111**, 110503 (2013).

[37] E. Shchukin and P. van Loock, Generalized conditions for genuine multipartite continuous-variable entanglement, Phys. Rev. A **92**, 042328 (2015).

[38] S. Gerke, J. Sperling, W. Vogel, Y. Cai, J. Roslund, N. Treps, and C. Fabre, Full Multipartite Entanglement of Frequency-Comb Gaussian States, Phys. Rev. Lett. **114**, 050501 (2015).

[39] S. Gerke, J. Sperling, W. Vogel, Y. Cai, J. Roslund, N. Treps, and C. Fabre, Multipartite Entanglement of a Two-Separable State, Phys. Rev. Lett. **117**, 110502 (2016).

[40] A. Roy and M. Devoret, Introduction to parametric amplification of quantum signals with Josephson circuits, C. R. Phys. **17**, 740 (2016).

[41] See Supplemental Material at http://link.aps.org/supplemental/10.1103/PhysRevLett.130.120601 for further details regarding the measurement setup, sample design, data analysis and theoretical model.

[42] Intermodulation products, https://intermodulation-products.com/, Accessed: 2021-10-19.

[43] E. A. Tholén, D. Platz, D. Forchheimer, V. Schuler, M. O. Tholén, C. Hutter, and D. B. Haviland, Note: The intermodulation lockin analyzer, Rev. Sci. Instrum. **82**, 026109 (2011).

[44] Multifrequency lockin basics, https://www.intermod.pro/manuals/IMP-MLA_user_manual/lockin.html, Accessed: 2022-11-13.

[45] S. W. Jolin, R. Borgani, M. O. Tholén, D. Forchheimer, and D. B. Haviland, Calibration of mixer amplitude and phase imbalance in superconducting circuits, Rev. Sci. Instrum. **91**, 124707 (2020).

[46] M. Mariantoni, E. P. Menzel, F. Deppe, M. A. Araque Caballero, A. Baust, T. Niemczyk, E. Hoffmann, E. Solano, A. Marx, and R. Gross, Planck Spectroscopy and Quantum Noise of Microwave Beam Splitters, Phys. Rev. Lett. **105**, 133601 (2010).

[47] E. Tholén, Intermodulation in microresonators for microwave amplification and nanoscale surface analysis, Ph.D. thesis, KTH, Sweden, 2009.

[48] A. A. Clerk, M. H. Devoret, S. M. Girvin, F. Marquardt, and R. J. Schoelkopf, Introduction to quantum noise, measurement, and amplification, Rev. Mod. Phys. **82**, 1155 (2010).

[49] C. M. Caves, Quantum limits on noise in linear amplifiers, Phys. Rev. D **26**, 1817 (1982).

[50] A. Pastore, An introduction to bootstrap for nuclear physics, J. Phys. G **46**, 052001 (2019).

[51] S. Diamond and S. Boyd, CVXPY: A Python-embedded modeling language for convex optimization, J. Mach. Learn. Res. **17**, 1 (2016), http://jmlr.org/papers/v17/15-408.html.

[52] A. Agrawal, R. Verschueren, S. Diamond, and S. Boyd, A rewriting system for convex optimization problems, J. Control Decision **5**, 42 (2018).

[53] scipy.optimize.differential_evolution, https://docs.scipy.org/doc/scipy/reference/generated/scipy.optimize.differential_evolution.html, Accessed: 2022-09-11.

[54] scipy.stats.kurtosistest, https://docs.scipy.org/doc/scipy/reference/generated/scipy.stats.kurtosistest.html, Accessed: 2022-07-19.

[55] scipy.stats.skewtest, https://docs.scipy.org/doc/scipy/reference/generated/scipy.stats.skewtest.html, Accessed: 2022-07-19.

[56] C. W. Gardiner and M. J. Collett, Input and output in damped quantum systems: Quantum stochastic differential equations and the master equation, Phys. Rev. A **31**, 3761 (1985).

[57] Y. Hong and S. Luo, Detecting k-nonseparability via local uncertainty relations, Phys. Rev. A **93**, 042310 (2016).

[58] M. Huber, F. Mintert, A. Gabriel, and B. C. Hiesmayr, Detection of High-Dimensional Genuine Multipartite Entanglement of Mixed States, Phys. Rev. Lett. **104**, 210501 (2010).

[59] L. K. Shalm, D. R. Hamel, Z. Yan, C. Simon, K. J. Resch, and T. Jennewein, Three-photon energy–time entanglement —Nature Physics, Nat. Phys. **9**, 19 (2013).

[60] R. Y. Teh and M. D. Reid, Criteria for genuine N-partite continuous-variable entanglement and Einstein-Podolsky-Rosen steering, Phys. Rev. A **90**, 062337 (2014).

[61] O. Gühne and G. Tóth, Entanglement detection, Phys. Rep. **474**, 1 (2009).

[62] T. Aoki, N. Takei, H. Yonezawa, K. Wakui, T. Hiraoka, A. Furusawa, and P. van Loock, Experimental Creation of a Fully Inseparable Tripartite Continuous-Variable State, Phys. Rev. Lett. **91**, 080404 (2003).

[63] A. Serafini, *Quantum Continuous Variables: A Primer of Theoretical Methods* (Taylor & Francis, Andover, England, UK, 2017).

[64] P. Hyllus and J. Eisert, Optimal entanglement witnesses for continuous-variable systems, New J. Phys. **8**, 51 (2006).

[65] L.-Y. Qu, J. Cotler, F. Ma, J.-Y. Guan, M.-Y. Zheng, X. Xie, Y.-A. Chen, Q. Zhang, F. Wilczek, and J.-W. Pan, Color Erasure Detectors Enable Chromatic Interferometry, Phys. Rev. Lett. **123**, 243601 (2019).

[66] X.-L. Wang, L.-K. Chen, W. Li, H.-L. Huang, C. Liu, C. Chen, Y.-H. Luo, Z.-E. Su, D. Wu, Z.-D. Li, H. Lu, Y. Hu, X. Jiang, C.-Z. Peng, L. Li, N.-L. Liu, Y.-A. Chen, C.-Y. Lu, and J.-W. Pan, Experimental Ten-Photon Entanglement, Phys. Rev. Lett. **117**, 210502 (2016).

[67] C. Weedbrook, S. Pirandola, R. García-Patrón, N. J. Cerf, T. C. Ralph, J. H. Shapiro, and S. Lloyd, Gaussian quantum information, Rev. Mod. Phys. **84**, 621 (2012).

[68] E. Shchukin and P. van Loock, Recovering Quantum Properties of Continuous-Variable States in the Presence of Measurement Errors, Phys. Rev. Lett. **117**, 140504 (2016).

[69] R. Simon, Peres-Horodecki Separability Criterion for Continuous Variable Systems, Phys. Rev. Lett. **84**, 2726 (2000).

[70] L.-M. Duan, G. Giedke, J. I. Cirac, and P. Zoller, Inseparability Criterion for Continuous Variable Systems, Phys. Rev. Lett. **84**, 2722 (2000).

[71] M. Seevinck and J. Uffink, Partial separability and entanglement criteria for multiqubit quantum states, Phys. Rev. A **78**, 032101 (2008).

[72] W. Dür and J. I. Cirac, Classification of multiqubit mixed states: Separability and distillability properties, Phys. Rev. A **61**, 042314 (2000).

[73] R. Y. Teh and M. D. Reid, Criteria to detect genuine multipartite entanglement using spin measurements, Phys. Rev. A **100**, 022126 (2019).

[74] F. Arzani, C. Fabre, and N. Treps, Versatile engineering of multimode squeezed states by optimizing the pump spectral profile in spontaneous parametric down-conversion, Phys. Rev. A **97**, 033808 (2018).

[75] F. Lecocq, L. Ranzani, G. A. Peterson, K. Cicak, R. W. Simmonds, J. D. Teufel, and J. Aumentado, Nonreciprocal Microwave Signal Processing with a Field-Programmable Josephson Amplifier, Phys. Rev. Appl. **7**, 024028 (2017).

[76] J. S. Hung, J. Busnaina, C. S. Chang, A. Vadiraj, I. Nsanzineza, E. Solano, H. Alaeian, E. Rico, and C. Wilson, Quantum Simulation of the Bosonic Creutz Ladder with a Parametric Cavity, Phys. Rev. Lett. **127**, 100503 (2021).

[77] A. McDonald, T. Pereg-Barnea, and A. A. Clerk, Phase-Dependent Chiral Transport and Effective Non-Hermitian Dynamics in a Bosonic Kitaev-Majorana Chain, Phys. Rev. X **8**, 041031 (2018).

[78] J. Nokkala, R. Martínez-Peña, G. L. Giorgi, V. Parigi, M. C. Soriano, and R. Zambrini, Gaussian states of continuous-variable quantum systems provide universal and versatile reservoir computing, Commun. Phys. **4**, 53 (2021).